NASA TECHNICAL NOTE

NASA TN D-5939

AN ADAPTIVE CONTROLLER FOR SPACE BASE SPIN PLANE ORIENTATION

by Willard W. Anderson and Ralph W. Will

Langley Research Center
Hampton, Va. 23365

NATIONAL AERONAUTICS AND SPACE ADMINISTRATION • WASHINGTON, D. C. • AUGUST 1970

1. Report No.	2. Government Accession No.	3. Recipie.
NASA TN D-5939		

4. Title and Subtitle	5. Report Date
AN ADAPTIVE CONTROLLER FOR SPACE BASE SPIN PLANE ORIENTATION	August 1970
	6. Performing Organization Code
7. Author(s)	8. Performing Organization Report No.
Willard W. Anderson and Ralph W. Will	L-7157
	10. Work Unit No.
9. Performing Organization Name and Address	125-19-10-06
NASA Langley Research Center Hampton, Va. 23365	11. Contract or Grant No.
	13. Type of Report and Period Covered
12. Sponsoring Agency Name and Address	Technical Note
National Aeronautics and Space Administration Washington, D.C. 20546	14. Sponsoring Agency Code

15. Supplementary Notes

16. Abstract

An adaptive attitude control system for the precise earth orientation of an artificial-gravity space base is presented. The adaptive logic forms a performance index based on the control torques required to hold a constant orientation with respect to the orbit plane in the presence of environmental torques. The adaptive control system acts to minimize this performance index and thus acquires an orientation with respect to the orbit plane where the environmental disturbance bias torques precess the space base at the orbit regression rate. This precession permits the space base to operate at a fixed orientation with respect to the orbit plane with no requirement for steady-state attitude-control fuel. It is also shown that this condition is stable and that any angular offset from this point results in a stable coning motion of the space base spin axis with respect to the orbit plane. Simulation results are presented for both the adaptive control system performance and the space base motions.

17. Key Words (Suggested by Author(s))	18. Distribution Statement
Space base Adaptive controller Spin-plane orientation	Unclassified – Unlimited

19. Security Classif. (of this report)	20. Security Classif. (of this page)	21. No. of Pages	22. Price*
Unclassified	Unclassified	36	$3.00

*For sale by the Clearinghouse for Federal Scientific and Technical Information
Springfield, Virginia 22151

AN ADAPTIVE CONTROLLER FOR SPACE BASE SPIN PLANE ORIENTATION

By Willard W. Anderson and Ralph W. Will
Langley Research Center

SUMMARY

An adaptive attitude control system for the precise earth orientation of an artificial-gravity space base is presented. The adaptive logic forms a performance index based on the control torques required to hold a constant orientation with respect to the orbit plane in the presence of environmental torques. The adaptive control system acts to minimize this performance index and thus acquires an orientation with respect to the orbit plane where the environmental disturbance bias torques precess the space base at the orbit regression rate. This precession permits the space base to operate at a fixed orientation with respect to the orbit plane with no requirement for steady-state attitude-control fuel. It is also shown that this condition is stable and that any angular offset from this point results in a stable coning motion of the space base spin axis with respect to the orbit plane. Simulation results are presented for both the adaptive control system performance and the space base motions.

INTRODUCTION

Manned orbiting space base concepts, such as that shown in figure 1, involve large rotating elements for artificial-gravity modules and zero-gravity hub modules for engineering and scientific experiments. Pointing experiments such as astronomical telescopes and earth resource packages require that the zero-gravity hub and thus the rotating element spin axis be stabilized. Arbitrary pointing and stabilization of the spacecraft spin or momentum vector require significant amounts of reaction jet fuel or prohibitively large momentum storage devices because of the extremely large angular momentum associated with the space base rotating element. A method of stabilizing the space base by utilizing the external gravity gradient and aerodynamic disturbances would eliminate the need for continuous attitude control.

One means of achieving such space base passive stabilization is to tilt the rotating element momentum vector out of the orbit plane so that the bias components of the external disturbances would precess the spacecraft at the orbit regression rate and therefore maintain a constant orientation with respect to the orbit plane. Selection of the proper

spacecraft orientation for this operation would be accomplished by a relatively simple adaptive controller. The initial acquisition using adaptive control techniques would be made by using reaction jets to maneuver the entire space base. After acquisition, base control would be possible by use of a control moment gyro (CMG) system mounted in the nonrotating element. The authors wish to acknowledge parallel efforts of K. L. Lindsay of Manned Spacecraft Center.

These considerations were used to synthesize adaptive control logic, an adaptive system performance index, and a space base control law to acquire the proper orientation for passive control of the space base.

SYMBOLS

A	matrix of direction cosines
a	arbitrary maneuver magnitude
a_{ij}	matrix elements
C_1, C_2, C_3	quasi-linear constants
D	maximum drag force
E	single-rotation matrix
F	aerodynamic drag force
G	unit bias torque
H	angular momentum
I	principal inertia
i	orbit inclination
J	gravity gradient torque
K	adaptive controller gain
k	local-vertical direction cosines

L	aerodynamic torque
l	longitude
$\dot{l}$	orbit precession rate
N	space base spin rate
r_{cp}	center-of-pressure coordinate
T	body torque
t	time
$\bar{u}$	unit vector
X,Y,Z	coordinate axes
x	state variable
δ	stopping condition bound
ϵ	equatorial-ecliptic inclination
ξ	complex coning vector
ρ	performance index
τ	orbit period
τ_c	time constant
ϕ,θ,ψ	Euler angle set
ϕ^*,θ^*,ψ^*	low-frequency Euler angle set
ϕ_o^*	base-spin-vector offset angle
ϕ_o^{**}	base-spin-vector cone angle

Ω	orbit angular rate
Ω_b	spin frequency
Ω_o	linear base precession frequency
ω	base body rate

Subscripts:

a	actual data
b	body
c	control
d	aerodynamic drag
h	heliocentric
i	inertial
o	orbit
s	sun
v	local vertical
x,y,z	axes of space base

Conventions:

$[\ ]$	matrix
$\{\ \}$	column matrix or vector
$\lvert\ \rvert$	absolute value
∇	vector gradient operator

Δ change in a variable

$\langle\ \rangle$ average value for one base revolution

$\langle\langle\ \rangle\rangle$ average value for one base orbit

Bars over symbols denote vectors. Dots over symbols denote derivatives with respect to time. Primed symbols denote spatial derivatives.

SPACE BASE AND CONTROL SYSTEM CONFIGURATION

Figure 1 shows a possible space base configuration to house 50 to 100 men and a scientific laboratory in the 1980 time period. The space base shown consists of two basic elements: a rotating artificial-gravity living quarters section ("disk") and a zero-gravity hub which contains all pointing experiments and the logistics system docking facilities. The two elements are connected by a low-frequency spring system contained in the compliant hub module which isolates the hub and its critical pointing experiments from the disturbances due to wobbling and imbalance of the rotating section. The spring mechanism also allows the hub to be maneuvered with respect to the rotating element spin axis and is sized so that the natural frequencies of the two rigid-body systems lie above the gravity gradient cyclic frequency (twice orbit frequency) but below the rotational frequency. Therefore, the bodies behave as a single rigid body from the cyclic gravity gradient point of view but the hub is isolated from the higher frequency "disk" rotation inputs.

The zero-gravity hub is stabilized and pointed by a control-moment-gyro (CMG) system. This orientation method includes rolling the entire hub about the base spin axis to provide a second degree of freedom for the solar cell array and solar experiments module. The pointing experiments are mounted on individual gimbaled platforms which provide the precise stabilization involved and the pointing capability with respect to the hub required to work with various targets such as the earth's surface, the sun, and stellar phenomena. A large space shuttle vehicle (12-man capacity) could be docked to the end of the hub module and would represent the most radical change in configuration inertia, and associated gravity gradient disturbances experienced by the base during normal operation.

The rotating section of the space base is controlled and reoriented by a reaction jet system located on the ends of the 200-foot rotating arms. The reaction jets are pulse-modulated to fire during parts of the spin cycle as shown in figure 2 to produce torques about particular axes. It should be noted that the firing regions in figure 2 are referenced to the "low-frequency body axes" corresponding to the system with respect to which the base is controlled. When the rotating base arms are within these regions, the jets

may be fired for the proper amount of time and in the proper sense to produce the desired precession rate for reorientation or control.

Physical System Description

The basic coordinate system used for inertial reference is a geocentric equatorial coordinate system X_i,Y_i,Z_i and is shown in figure 3. The X_i-axis is arbitrarily chosen to pass through the vernal equinox. This axis is collinear with the X_h-axis of a heliocentric ecliptic coordinate system X_h,Y_h,Z_h, the rotation about the X-axis being the equatorial-ecliptic inclination ϵ ($\epsilon \approx 23.5^o$). A sun-line unit vector $\bar{u}_s$ is defined by the heliocentric longitude l_s. The space base orbit plane X_o,Y_o is also shown; it is defined by the equatorial longitude l and the orbit inclination i. Orbit precession $\dot{l}$ is taken as -4.5^o per day for an inclination of 55^o and a circular orbit of 250 nautical miles (463 km). (See ref. 1.) Space base attitude, relative to the orbit coordinate system, is defined by the Euler angle set ϕ_o,θ_o,ψ_o for the 1,2,3 rotation sequence in figure 4. Space base position in orbit is given by the orbit plane longitude l_b. Also illustrated in figure 4 are a local vertical unit vector $\bar{u}_v$ and a free-stream air velocity unit vector $\bar{u}_d$.

Space base attitudes relative to orbit coordinates are required for control purposes but are not an inertial set, since the orbit regresses. A second set of Euler angles ψ_i,θ_i,ϕ_i for a 3,2,1 rotation sequence, relative to the geocentric equatorial coordinate system, is used to describe the physical system. These Euler angles are found by assuming the space base spin momentum magnitude to be constant for the range of frequencies considered and by solving the following statement of conservation of angular momentum:

$$\bar{T}_b = \bar{\omega}_b \times \bar{H} \tag{1}$$

where $\bar{T}_b$ is the total body torque, $\bar{\omega}_b$ is the body rate, and $\bar{H}$ is the constant magnitude spin momentum. This formulation excludes the higher frequency dynamics associated with base flexibility, rotation, and nutation, but does give an accurate low-frequency characterization of an actual space base provided the spin momentum is large and remains alined with the Z_b-axis. The body rates found by solution of equation (1) are transformed to Euler rates and integrated to yield the set ψ_i,θ_i,ϕ_i. The transformation of body rates to Euler rates, taken from reference 2, is

$$\left.\begin{aligned} \dot{\psi}_i &= \frac{\omega_y \sin \phi_i + \omega_z \cos \phi_i}{\cos \theta_i} \\ \dot{\theta}_i &= \omega_y \cos \phi_i - \omega_z \sin \phi_i \\ \dot{\phi}_i &= \omega_x + \dot{\psi}_i \sin \theta_i \end{aligned}\right\} \tag{2}$$

The Euler angle set ϕ_o,θ_o,ψ_o are found by taking the matrix of direction cosines defining the body in inertial coordinates $[A_{bi}]$ and transforming it to a matrix of direction cosines defining the body in orbit coordinates $[A_{bo}]$. The elements of this matrix can be used to solve for the three Euler angles as shown in appendix A. (See ref. 3.)

The environmental torques considered in this report are gravity gradient torques and aerodynamic torques. These torques are derived in appendix B and their final form excludes the "high" frequency components associated with base revolution. From appendix B, the gravity-gradient torques in body coordinates are

$$\left.\begin{aligned} \langle J_x \rangle &= -3\Omega^2 k_y k_z \left(\langle I_{x,y} \rangle - I_z \right) \\ \langle J_y \rangle &= -3\Omega^2 k_x k_z \left(I_z - \langle I_{x,y} \rangle \right) \\ \langle J_z \rangle &= 0 \end{aligned}\right\} \tag{3}$$

where

$$\{k\} = [A_{bo}]\{u_v\}$$

$$\langle I_{x,y} \rangle = \frac{I_x + I_y}{2}$$

The aerodynamic torques, also in body coordinates, from appendix B are

$$\left.\begin{aligned} \langle L_x \rangle &= r_{cp,y} F_z - r_{cp,z} F_y \\ \langle L_y \rangle &= r_{cp,z} F_x - r_{cp,x} F_z \\ \langle L_z \rangle &= r_{cp,x} F_y - r_{cp,y} F_x \end{aligned}\right\} \tag{4}$$

where

$$\{F\} = \{\langle D \rangle\}^T [A_{bo}] \{u_d\}$$

Of these two sets of environmental torques, only the gravity-gradient torques are assumed to have steady-state components (bias). These bias torques can be shown to vary linearly with body-to-orbit attitude, for small body-to-orbit angles, and for the example configuration of this report can be characterized as follows (appendix B, eqs. (B7)):

$$\left.\begin{aligned} \langle\langle J_x \rangle\rangle &\approx -G\phi_o \\ \langle\langle J_y \rangle\rangle &\approx -G\theta_o \\ \langle\langle J_z \rangle\rangle &\approx 0 \\ G &\approx \frac{3}{2}\Omega^2 \left(I_z - \langle I_{x,y} \rangle \right) \end{aligned}\right\} \tag{5}$$

The following linear (small ϕ_o,θ_o,ψ_o) analysis is included to characterize the passive coning of the space base spin vector in terms of angle and frequency.

It is is assumed that ψ_o is initially zero and remains so since $\langle\langle J_z \rangle\rangle \approx 0$, referring to figure 5, the X_b-axis and Y_b-axis body rates are

$$\left.\begin{aligned} \omega_x &= \frac{G\theta_o}{H} \\ \omega_y &= -\frac{G\phi_o}{H} \end{aligned}\right\} \tag{6}$$

The orbit plane regression rate components along the X_b-axis and Y_b-axis are zero and $\dot{i} \sin(i + \phi_o)$, respectively. Transforming these rates to find rates for the body relative to orbit yields

$$\left.\begin{aligned} \phi_o &= \frac{G\theta_o}{H} \\ \dot{\theta}_o &= -\dot{i} \sin(i + \phi_o) - \frac{G\phi_o}{H} \end{aligned}\right\} \tag{7}$$

or expanding $(\sin i + \phi_o)$ and rewriting yields

$$\left.\begin{aligned} \ddot{\phi}_o + \Omega_o^2 \phi_o &= \Omega_o^2 \phi_o^* \\ \theta_o &= \frac{H}{G} \dot{\phi}_o \end{aligned}\right\} \tag{8}$$

where

$$\left.\begin{aligned} \phi_o^* &= -\frac{H\dot{i} \sin i/G}{1 + \frac{H\dot{i} \cos i}{G}} \\ \Omega_o &= \frac{G\left(1 + \frac{H\dot{i}C_i}{G}\right)^{1/2}}{H} \end{aligned}\right\} \tag{9}$$

A complex solution to equations (8) for an arbitrary set of initial conditions $(\phi_o(0), \theta_o(0))$, valid when $\Omega_o >> |\dot{i} \cos i|$ or $|H\dot{i}C_i/G| << 1$, is shown in figure 6 where

$$\xi = \phi_o^* + \phi_o^{**} e^{-i\Omega_o t} \tag{10}$$

and where

$$\phi_o^{**} = \left\{\left[\phi_o(0) - \phi_o^*\right]^2 + \left[\theta_o(0)\right]^2\right\}^{1/2}$$

This relationship means that, within the stated assumptions, a space base spin vector will cone about an axis which is stationary relative to the regressing orbit plane, the angle and period of coning being given by ϕ_o^{**} and Ω_o, respectively. This report

describes a steepest descent adaptive controller with and without learning the type that would be utilized on a spinning space base to seek out and aline the base with the stationary vector and, thus, maintain the base with a fixed attitude relative to its orbit plane, without the use of steady-state fuel.

Control System Description

The function of the adaptive controller (fig. 7) is to find that space base orbit orientation where no control torques (fuel) are required to maintain the orientation. The adaptive controller performance index ρ must thus be defined as a function of control torques which, in turn, are functions of the orientation angles. The problem is reduced to two degrees of freedom, since the spinning space base considered averages out the X_b-axis and Y_b-axis inertia difference. (See appendix B.) However, to insure a two-degree-of-freedom problem, a Z_b-axis controller is used to maintain ψ_o at zero. The performance index ρ is an even function of the average X_b-axis and Y_b-axis control torques for one-half orbit. The half-orbit does remove the influence of cyclic gravity-gradient components, since their period is one-half orbit, but it does not necessarily remove the influence of cyclic aerodynamic torques, since their period is an entire orbit. The shorter time period is obviously desirable and no adverse effect from using it occurred during simulation. The index is defined as

$$\rho\left(\phi_o,\theta_o\right) = \langle T_{c,x}\rangle^2 + \langle T_{c,y}\rangle^2 \tag{11}$$

where

$$\langle T_{c,x}\rangle = \frac{2}{\tau}\int_0^{\tau/2} T_{c,x}\,dt$$

$$\langle T_{c,y}\rangle = \frac{2}{\tau}\int_0^{\tau/2} T_{c,y}\,dt$$

and τ is the orbit period.

The performance index ρ is measured by holding the base at a fixed orientation and computing the integrals of the torques required to hold that orientation. If the attitude control system errors are small during this period, these integrals represent an accurate measurement of the external surface and body torques acting on the base, the components of torques required to maintain orbit regression rate not being included. By orienting the base with a single-degree-of-freedom maneuver (for example, ϕ_o) and remeasuring ρ, an estimate of the variation of ρ with this degree of freedom (for example, $\partial\rho/\partial\phi_o$) is found. A similar maneuver for the remaining degree of freedom θ_o allows an estimate of $\partial\rho/\partial\theta_o$. The two maneuvers allow an estimate of $\nabla\rho$. An adaptive control technique is to allow these maneuvers to have amplitudes which are proportional to the measured gradients. This method is called the method of steepest descent. (See ref. 4.) The successive orientations are thus

$$x_{new} = x_{old} - K \nabla\rho \tag{12}$$

where

$$x = \begin{Bmatrix} \phi_o \\ \theta_o \end{Bmatrix}$$

A stopping condition is met when $|\nabla\rho|^2$ is less than a fixed amount δ. No constraint boundaries are included and the gain K is held constant.

The maneuver and hold logic used first computes desired Euler rates from the new Euler command angles

$$\left.\begin{aligned} \dot{\phi}_{o,c} &= \frac{1}{\tau_c}\left(\phi_{o,new} - \phi_o\right) \\ \dot{\theta}_{o,c} &= \frac{1}{\tau_c}\left(\theta_{o,new} - \theta_o\right) \\ \dot{\psi}_{o,c} &= \frac{1}{\tau_c}\left(-\psi_o\right) \end{aligned}\right\} \tag{13}$$

and then converts these angles to body rates

$$\left.\begin{aligned} \omega_{x,c} &= \dot{\phi}_{o,c} \cos\dot{\theta}_o \cos\psi_o + \dot{\theta}_{o,c} \sin\psi_o \\ \omega_{y,c} &= \dot{\theta}_{o,c} \cos\psi_o - \dot{\phi}_{o,c} \cos\theta_o \sin\psi_o \\ \omega_{z,c} &= \dot{\psi}_{o,c} + \dot{\phi}_{o,c} \sin\theta_o \end{aligned}\right\} \tag{14}$$

and commands the base reaction control system to produce these body rates. The system continues this iterative motion until the stopping condition is met.

The steepest descent logic, as outlined, operates from point to point in state vector space and does not retain information prior to the previous iteration. A learning procedure was included to use prior information in order to reduce the time required to reach the steady-state orientation. Past maneuver amplitudes are used to form two Taylor series expansions from which future maneuver amplitudes $\left(\Delta\phi_{o,c}, \Delta\theta_{o,c}\right)$ can be estimated. These two Taylor series are both solved iteratively for a point of minimum ρ (no commanded maneuver) near a point determined by linear extrapolation only. These expansions for command maneuvers are

$$\left.\begin{aligned} 0 &= \Delta\phi_{o,a} + \Delta\phi'_{o,a}\left(\Delta\phi_{o,c}\right) + \frac{\Delta\phi''_{o,a}\left(\Delta\phi_{o,c}\right)^2}{2!} + \frac{\Delta\phi'''_{o,a}\left(\Delta\phi_{o,c}\right)^3}{3!} + \cdots \\ 0 &= \Delta\theta_{o,a} + \Delta\theta'_{o,a}\left(\Delta\theta_{o,c}\right) + \frac{\Delta\theta''_{o,a}\left(\Delta\theta_{o,c}\right)^2}{2!} + \frac{\Delta\theta'''_{o,a}\left(\Delta\theta_{o,c}\right)^3}{3!} + \cdots \end{aligned}\right\} \tag{15}$$

where the primes denote approximate spatial derivatives.

An algorithm is used to compute and test successive maneuvers for appropriate stability during the initial steepest descent iterations and when these maneuvers meet certain stability tests, ϕ_o and θ_o maneuvers are commanded according to the solutions of equations (15). After acquisition of this assumed point of minimum ρ, the method of steepest descent logic is used to maneuver to within the stopping condition bounds of the exact point of minimum ρ.

SIMULATION RESULTS

The space base low-frequency dynamics, low-frequency environmental torques, coordinate transformations, and adaptive control logic were programed on a Control Data 6600 digital computer. Table I includes a summary of assumed inertia, spin rate, and angular momentum characteristics of the example space base configurations considered during the simulation. Also shown in table I are the offset angles and frequencies predicted by the linear analysis (eqs. (9)) for the four configurations, and their agreement with simulation runs.

TABLE I.- EXAMPLE CONFIGURATION SUMMARY

[$i = 55^o$; $\dot{i} = -4.5^o$/day; altitude, 250 nautical miles (463 km)]

Case	$\langle I_{x,y} \rangle$		I_z		N, rpm	H		ϕ_o^*, deg		Ω_o, rad/sec	
	slug-ft^2	kg-m^2	slug-ft^2	kg-m^2		ft-lb-sec	N-m-sec	Linear	Simulation	Linear	Simulation
Low speed	193×10^6	262×10^6	320×10^6	434×10^6	0.2	6.75×10^6	9.15×10^6	1.133	1.15	38 $\times 10^{-6}$	36.2 $\times 10^{-6}$
Design	193	262	320	434	2.0	67.5	91.5	12.95	13.0	3.55	3.09
Shuttle docked	243	330	320	434	2.0	67.5	91.5	23.60	25.1	2.03	*.89
Growth version	353	479	640	868	2.0	135	183	11.28	11.4	4.03	3.59

*Dynamics are too nonlinear for agreement.

The space base design configuration rotates at 2 revolutions per minute to produce 0.25g at the center line of the living quarters module. The low speed configuration represents the basic space base spinning at 0.2 revolution per minute. This case was considered to demonstrate that the adaptive logic is not sensitive to spin speed for a particular inertia configuration. A docked shuttle spacecraft adds an inertia load of 50×10^6 slug-ft^2 (68×10^6 kg-m^2) to the space base X- and Y-axes (Z-axis change neglected) and represents a radically different inertia distribution. The growth version of the space base consists of four rotating arms rather than two for the design configuration. This configuration would represent a total increase in base crew contingent or power generation capability.

Typical simulation output is shown in figure 8, which is a time history of space base attitudes and environmental and control torques for the 0.2-rpm acquisition case of figure 9. The spacecraft attitudes ϕ_o and θ_o are measured with respect to the orbit plane as defined in figure 4. Also shown are the gravity-gradient disturbance

torques which are referenced to the space base body axes. The orbit precession angle and the control system torques are also shown. A corresponding cross-axis trace of the spin axis angles, ϕ_o and θ_o, with respect to the orbit plane is shown in figure 9. This trace was generated simultaneously with figure 8. The spin axis started normal to the orbit plane $\left(\phi_o(0) = \theta_o(0) = 0\right)$ and was allowed to precess under the external disturbances. The motion agrees well with the linear prediction represented in figure 6, measured values of ϕ_o^* and Ω_o agreeing to within 5 percent of the linear predictions of table I. The cyclic gravity-gradient disturbances (at twice orbit frequency) are shown on the higher speed sections of figure 8 and their influence on base motion is evident on the cross-axis trace. The adaptive system was then activated and started to acquire the point where the external disturbance bias will maintain the base orientation constant with respect to the precessing orbit. The control torques during this period are low-level cyclic torques required to counteract the external disturbances and high-level step torques required to perform the reorientation maneuvers commanded by the adaptive logic. The adaptive logic may be terminated at any point as shown in figure 9 and the spacecraft allowed to precess with the resulting error or coning angle decrease. The adaptive control system was reactivated and completed the acquisition of the desired orientation. The system was shut off automatically when the stopping condition was met. The external disturbances again precess the spacecraft in a small cone with respect to the orbit plane, the cone angle being a direct function of the stopping condition. Superimposed on this low-frequency coning motion is the precession caused by the cyclic gravity-gradient and aerodynamic disturbances.

Figure 10 shows a cross-axis trace for a similar run involving the 2-rpm design space base configuration. This configuration, having ten times more angular momentum, is precessed through approximately ten times the previous cone angle by the external disturbances. The measured values of ϕ_o^* and Ω_o agreed to within 13 percent of those listed in table I. The only modification to the adaptive system for the 2.0-rpm configuration required was a change in the initial maneuver angles from 0.1^o to 1^o. This change is necessary because the gradient is not as large for this case and requires a large angle for accurate measurement. Figure 11 shows adaptive control system acquisition for the 2-rpm case from a variety of initial conditions with respect to the orbit plane. No difficulty was experienced by the adaptive controller for these conditions.

The docking of a shuttle spacecraft to the space base, as shown in figure 1, will radically change the base inertia distribution, the external disturbance profile, and the orientation at which the spacecraft will be precessed at orbit precession rate by the external disturbances. Figure 12 shows a cross-axis trace involving the 2-rpm configuration where acquisition has been accomplished by the adaptive control system and a shuttle vehicle docking occurs which upsets the stable situation. The adaptive controller is left off for a period following the docking to illustrate that the external environment

will precess the spacecraft in a new cone. The measured value of ϕ_o^* agreed with that in table I; however, ϕ_o^* is too large for the linear analysis to predict Ω_o, where the measured value was approximately one-half that given in table I. However, when the adaptive system is activated, no difficulty is experienced in acquiring the new desired orientation with the combined configuration.

The growth version of the space base, which has four rotating arms as shown in figure 1, represents another extreme configuration variation for the adaptive control system. Acquisition of the desired orientation from a variety of initial conditions for this configuration is shown in figure 13. Values of ϕ_o^* and Ω_o measured agreed to within 11 percent with those of table I. Minor controller modifications, consisting of doubling the maximum reaction jet control torque level (using a second set of reaction jets located on the second set of arms) and decreasing the adaptive gain k in proportion to the increase in performance index, resulted from the increased inertia differences. This technique permitted the controller to accomplish acquisition without difficulty.

The simplicity, predictability, and reliability of the method of steepest adaptive controller are attractive; however, the number of orbits required to acquire the steady-state orientation is large and results in a large expenditure of fuel. For the design configuration acquisitions shown in figure 11, the average fuel consumption was approximately 850 lbm (385 kg) (for an assumed specific impulse of 250 lbf-sec/lbm (2440 N-sec^2/kg)) whereas the average number of orbits was 70. Total spin-up fuel for this configuration was 1120 lbm (508 kg).

Figure 14 shows design case acquisitions using the learning procedure discussed previously. The acquisition sequence begins by establishing a steepest descent pattern. When the ratio of successive maneuvers meets a stability criterion of the control algorithm, the space base is maneuvered directly to the computed point of minimum ρ. The method of steepest descent logic is then reactivated, if required, and the base is maneuvered until the stopping condition is met. For the design case acquisitions shown in figure 14 the average number of orbits required was 50 which represents considerable improvement over identical initial condition runs without the learning procedure.

CONCLUDING REMARKS

In the preceding analysis, equations for the "low-frequency" space base dynamic system have been developed and the system simulated. The results of this analysis and the simulation runs allow certain concluding remarks concerning the behavior of the system, within the boundaries of all connected simplifying assumptions.

First, the basic uncontrolled precession of the space base, with respect to the regressing orbit, resulting from the bias components of the gravity torques describes

a stable cone of predictable amplitude, offset, and frequency. Superimposed on this basic motion is the stable base coning resulting from the cyclic gravity gradient and aerodynamic torques.

Secondly, a simple and inherently reliable method of steepest descent adaptive controller has been synthesized and simulated which will acquire that axis in orbit space which minimizes the passive gravity-gradient-bias coning to any desired level. The controller can be turned off when the desired orientation is reached and no further expenditure of fuel is required.

Finally, the benefits of a simple learning technique have been demonstrated to illustrate the reduction of time and fuel that is possible if the complexity of the control algorithms is not limited.

Langley Research Center,
National Aeronautics and Space Administration,
Hampton, Va., June 3, 1970.

APPENDIX A

COORDINATE SYSTEM TRANSFORMATIONS

Space base attitude relative to a noninertial orbit coordinate system is a required input for the adaptive control computer. The transformations for obtaining this information used in the simulation are summarized in this section. The simulation transformations are analogous to those required to transform an inertial reference unit's attitude output to an orbit reference for control purposes.

Given the space base inertial attitude as a set of 3,2,1 rotation sequence Euler angles of magnitude ψ_i, θ_i, and ϕ_i, respectively, and using the notation of reference 3, the matrix of direction cosines required to transform a body vector to an inertial vector is

$$A_{ib} = E_3(-\psi_i)\, E_2(-\theta_i)\, E_1(-\phi_i)$$

$$= \begin{bmatrix} \cos\theta_i \cos\psi_i & -\cos\phi_i \sin\psi_i + \sin\phi_i \sin\theta_i \cos\psi_i & \sin\phi_i \sin\psi_i + \cos\phi_i \sin\theta_i \cos\psi_i \\ \cos\theta_i \sin\psi_i & \cos\phi_i \cos\psi_i + \sin\phi_i \sin\theta_i \sin\psi_i & -\sin\phi_i \cos\psi_i + \cos\phi_i \sin\theta_i \sin\psi_i \\ -\sin\theta_i & \sin\phi_i \cos\theta_i & \cos\phi_i \cos\theta_i \end{bmatrix} \qquad \text{(A1)}$$

where

$$\{\,\}_i = [A_{ib}]\{\,\}_b$$

The matrix of direction cosines required to transform an inertial vector to an orbit vector is

$$A_{oi} = E_1(i)\, E_3(\ell)$$

$$= \begin{bmatrix} \cos\ell & \sin\ell & 0 \\ -\cos i \sin\ell & \cos i \cos\ell & \sin i \\ \sin i \sin\ell & -\sin i \cos\ell & \cos i \end{bmatrix} \qquad \text{(A2)}$$

where

$$\{\,\}_o = [A_{oi}]\{\,\}_i$$

The product of these two matrices $A_{ob} = A_{oi}A_{ib}$ yields the matrix of direction cosines to transform a body vector to an orbit vector. The inverse of this product, $A_{bo} = A_{ob}^T$

(or transpose since it is orthogonal) can be used to compute the orbit reference Euler angles shown in figure 4. This computation is accomplished by equating the matrix $A_{bo}(\phi_i,\theta_i,\psi_i,l,i)$ to the matrix $A_{bo}(\phi_o,\theta_o,\psi_o)$. This latter matrix is

$$A_{bo} = E_3(\psi_o)\, E_2(\theta_o)\, E_1(\phi_o)$$

$$= \begin{bmatrix} \cos\psi_o \cos\theta_o & \cos\psi_o \sin\theta_o \sin\phi_o + \sin\psi_o \cos\phi_o & -\cos\psi_o \sin\theta_o \cos\phi_o + \sin\psi_o \sin\phi_o \\ -\sin\psi_o \cos\theta_o & -\sin\psi_o \sin\theta_o \sin\phi_o + \cos\psi_o \cos\phi_o & \sin\psi_o \sin\theta_o \cos\phi_o + \cos\psi_o \sin\phi_o \\ \sin\theta_o & -\cos\theta_o \sin\phi_o & \cos\theta_o \cos\phi_o \end{bmatrix} \qquad \text{(A3)}$$

where

$$\{\}_b = [A_{bo}]\{\}_o$$

The following procedure for computing ψ_o, θ_o, and ϕ_o can be verified by inspection of equation (A3) or by referring to reference 3:

$$\psi_o = \tan^{-1}\frac{-a_{21}}{a_{11}}$$

$$S_1 = a_{13}\sin\psi_o + a_{23}\cos\psi_o$$

$$C_1 = a_{22}\cos\psi_o + a_{12}\sin\psi_o$$

$$S_2 = a_{31}$$

$$C_2 = a_{33}C_1 - a_{32}S_1$$

$$\phi_o = \tan^{-1}\frac{S_1}{C_1}$$

$$\theta_o = \tan^{-1}\frac{S_2}{C_2}$$

where the elements of A_{bo} are

$$a_{11} = \cos l \cos\theta_i \cos\psi_i + \sin l \cos\theta_i \sin\psi_i$$

$$a_{12} = -\cos i \sin l \cos\theta_i \cos\psi_i + \cos i \cos l \cos\theta_i \sin\psi_i - \sin i \sin\theta_i$$

$$a_{13} = \sin i \sin l \cos\theta_i \cos\psi_i - \sin i \cos l \cos\theta_i \sin\psi_i - \cos i \sin\theta_i$$

$$a_{21} = \cos l\left(-\cos \phi_i \sin \psi_i + \sin \phi_i \sin \theta_i \cos \psi_i\right) + \sin l\left(\cos \phi_i \cos \psi_i + \sin \phi_i \sin \theta_i \sin \psi_i\right)$$

$$a_{22} = -\cos i \sin l\left(-\cos \phi_i \sin \psi_i + \sin \phi_i \sin \theta_i \cos \psi_i\right) + \cos i \cos l\left(\cos \phi_i \cos \psi_i + \sin \phi_i \sin \theta_i \sin \psi_i\right) + \sin i \sin \phi_i \cos \theta_i$$

$$a_{23} = \sin i \sin l\left(-\cos \phi_i \sin \psi_i + \sin \phi_i \sin \theta_i \cos \psi_i\right) - \sin i \cos l\left(\cos \phi_i \cos \psi_i + \sin \phi_i \sin \theta_i \sin \psi_i\right) + \cos i\left(\sin \phi_i \cos \theta_i\right)$$

$$a_{31} = \cos l\left(\sin \phi_i \sin \psi_i + \cos \phi_i \sin \theta_i \cos \psi_i\right) + \sin l\left(-\sin \phi_i \cos \psi_i + \cos \phi_i \sin \theta_i \sin \psi_i\right)$$

$$a_{32} = -\cos i \sin l\left(\sin \phi_i \sin \psi_i + \cos \phi_i \sin \theta_i \cos \psi_i\right) + \cos i \cos l\left(-\sin \phi_i \cos \psi_i + \cos \phi_i \sin \theta_i \sin \psi_i\right) + \sin i \cos \phi_i \cos \theta_i$$

$$a_{33} = \sin i \sin l\left(\sin \phi_i \sin \psi_i + \cos \phi_i \sin \theta_i \cos \psi_i\right) - \sin i \cos l\left(-\sin \phi_i \cos \psi_i + \cos \phi_i \sin \theta_i \sin \psi_i\right) + \cos i\left(\cos \phi_i \cos \theta_i\right)$$

APPENDIX B

ENVIRONMENTAL TORQUES

The following set of gravity gradient body torques are from reference 5 and have been rewritten in the nomenclature of this report:

$$\left.\begin{aligned} J_x &= -3\Omega^2 k_y k_z (I_y - I_z) \\ J_y &= -3\Omega^2 k_x k_z (I_z - I_x) \\ J_z &= -3\Omega^2 k_x k_y (I_x - I_y) \end{aligned}\right\} \tag{B1}$$

where the direction cosines k_x, k_y, and k_z define the local vertical unit vector at the base center of mass in body coordinates, $\{k\} = [A_{bo}]\{u_v\}$.

Since the base rotation frequency is much greater than the orbit frequency, this contribution can be eliminated for the low-frequency cases considered as follows:

Expanding

$$\{k\} = [A_{bo}] \begin{Bmatrix} \cos l_b \\ \sin l_b \\ 0 \end{Bmatrix}$$

yields

$$\left.\begin{aligned} k_x &= \cos \psi_o (C_1) + \sin \psi_o (C_2) \\ k_y &= \cos \psi_o (C_2) - \sin \psi_o (C_1) \\ k_z &= C_3 \end{aligned}\right\} \tag{B2}$$

where

$$C_1 = \cos \theta_o \cos l_b + \sin \theta_o \sin \phi_o \sin l_b$$

$$C_2 = \cos \phi_o \sin l_b$$

$$C_3 = \sin \theta_o \cos l_b - \cos \theta_o \sin \phi_o \sin l_b$$

The terms C_1, C_2, and C_3 are considered to be constant for the period of one base rotation. Also the Z-axis attitude ψ_o is considered to have a low-frequency component (constant for one rotation) in addition to the rotation or spin component, or

$$\psi_o = \psi_o^* + \Omega_b t \tag{B3}$$

where Ω_b is the base spin velocity. By referring to figure 4, it is noted that ψ_o is the final Euler rotation, and thus can be manipulated without changing ϕ_o or θ_o, as is shown in figure 15. Rewriting the gravity gradient torques for the low-frequency body axes $\left(X_b^*, Y_b^*, Z_b^*\right)$, of figure 15 by using equations (B1), (B2), and (B3), averaging for one rotation of the body, and omitting the asterisks, yields

$$\left.\begin{aligned} \langle J_x \rangle &= -3\Omega^2\left(C_2 \cos \psi_o - C_1 \sin \psi_o\right)\left(C_3\right)\left(\langle I_{x,y} \rangle - I_z\right) \\ \langle J_y \rangle &= -3\Omega^2\left(+C_1 \cos \psi_o + C_2 \sin \psi_o\right)\left(C_3\right)\left(I_z - \langle I_{x,y} \rangle\right) \\ \langle J_z \rangle &= 0 \end{aligned}\right\} \tag{B4}$$

where

$$\langle I_{x,y} \rangle = \frac{I_x + I_y}{2}$$

From inspection of equations (B2), equations (B4) can be written as

$$\left.\begin{aligned} \langle J_x \rangle &= -3\Omega^2 k_y k_z\left(\langle I_{x,y} \rangle - I_z\right) \\ \langle J_y \rangle &= -3\Omega^2 k_x k_z\left(I_z - \langle I_{x,y} \rangle\right) \\ \langle J_z \rangle &= 0 \end{aligned}\right\} \tag{B5}$$

By assuming ψ_o to be zero and ϕ_o and θ_o to be small, equations (B4) simplify to

$$\left.\begin{aligned} \langle J_x \rangle &\approx -3\Omega^2\left(\theta_o \sin l_b \cos l_b - \phi_o \sin^2 l_b\right)\left(\langle I_{x,y} \rangle - I_z\right) \\ \langle J_y \rangle &\approx -3\Omega^2\left(\theta_o \cos^2 l_b - \phi_o \sin l_b \cos l_b\right)\left(I_z - \langle I_{x,y} \rangle\right) \\ \langle J_z \rangle &\approx 0 \end{aligned}\right\} \tag{B6}$$

If it is assumed also that ϕ_o and θ_o remain essentially constant during one-half orbit, then

$$\left.\begin{aligned} \langle\langle J_x \rangle\rangle &\approx -\frac{3}{2}\Omega^2\left(I_z - \langle I_{x,y} \rangle\right)\phi_o \\ \langle\langle J_y \rangle\rangle &\approx -\frac{3}{2}\Omega^2\left(I_z - \langle I_{x,y} \rangle\right)\theta_o \\ \langle\langle J_z \rangle\rangle &\approx 0 \end{aligned}\right\} \tag{B7}$$

Aerodynamic torques result when the center of pressure of a body does not coincide with the center of mass. If a vector in body coordinates $\bar{r}_{cp}$ defines the position of the center of pressure relative to the center of mass, then the torque resulting from an aerodynamic drag force $\bar{F}$ also written in body coordinates, will be

$$\bar{L} = \bar{r}_{cp} \times \bar{F}$$

The drag force $\bar{F}$ can be modeled as having a direction parallel to the free-stream air velocity and a magnitude proportional to the scalar product of a vector $\langle \bar{D} \rangle$ whose components are the averaged maximum drag forces along the low-frequency body axes, and the free-stream unit vector $\bar{u}_d$, transformed to body coordinates. A matrix equation expressing this relation is

$$\{\langle L \rangle\} = [r_{cp}]\{\langle D \rangle\}^T [A_{bo}]\{u_d\} \tag{B8}$$

Expanding equation (B8) yields

$$\left.\begin{aligned} \langle L_x \rangle &= r_{cp,y}F_z - r_{cp,z}F_y \\ \langle L_y \rangle &= r_{cp,z}F_x - r_{cp,x}F_z \\ \langle L_z \rangle &= r_{cp,x}F_y - r_{cp,y}F_x \end{aligned}\right\} \tag{B9}$$

where

$$F_x = \left[\cos \psi_o \cos \theta_o \sin l_b - \left(\cos \psi_o \sin \theta_o \sin \phi_o + \sin \psi_o \cos \phi_o\right)\cos l_b\right]\langle D_x \rangle$$

$$F_y = \left[-\sin \psi_o \cos \theta_o \sin l_b + \left(\sin \psi_o \sin \theta_o \sin \phi_o - \cos \psi_o \cos \phi_o\right)\cos l_b\right]\langle D_y \rangle$$

$$F_z = \left[\sin \theta_o \sin l_b + \cos \theta_o \sin \phi_o \cos l_b\right]\langle D_z \rangle$$

It should be noted that these aerodynamic torques averaged for one orbit are zero (if it is assumed that the orientation is constant, r_{cp} is constant, and that the average maximum drag forces D_x, D_y, and D_z are constant for the entire orbit), or

$$\langle\langle L_x \rangle\rangle = \langle\langle L_y \rangle\rangle = \langle\langle L_z \rangle\rangle = 0$$

REFERENCES

1. Cook, G. E.: Luni-Solar Perturbations of the Orbit of an Earth Satellite. Geophys. J., vol. 6, no. 3, Apr. 1962, pp. 271-291.

2. Kurzhals, Peter R.; and Grantham, Carolyn: A System for Inertial Experiment Pointing and Attitude Control. NASA TR R-247, 1966.

3. Meyer, George; Lee, Homer Q.; and Wehrend, William R., Jr.: A Method for Expanding a Direction Cosine Matrix Into an Euler Sequence of Rotations. NASA TM X-1384, 1967.

4. Eveleigh, Virgil W.: Adaptive Control and Optimization Techniques. McGraw-Hill Book Co., Inc., c.1967.

5. Schalkowski, S.; and Cooley, W. C.: Gravity Gradient Torques on a Sun-Oriented Space Station. TR-001 (Contract NASw 543), Exotech Inc., Dec. 20, 1962.

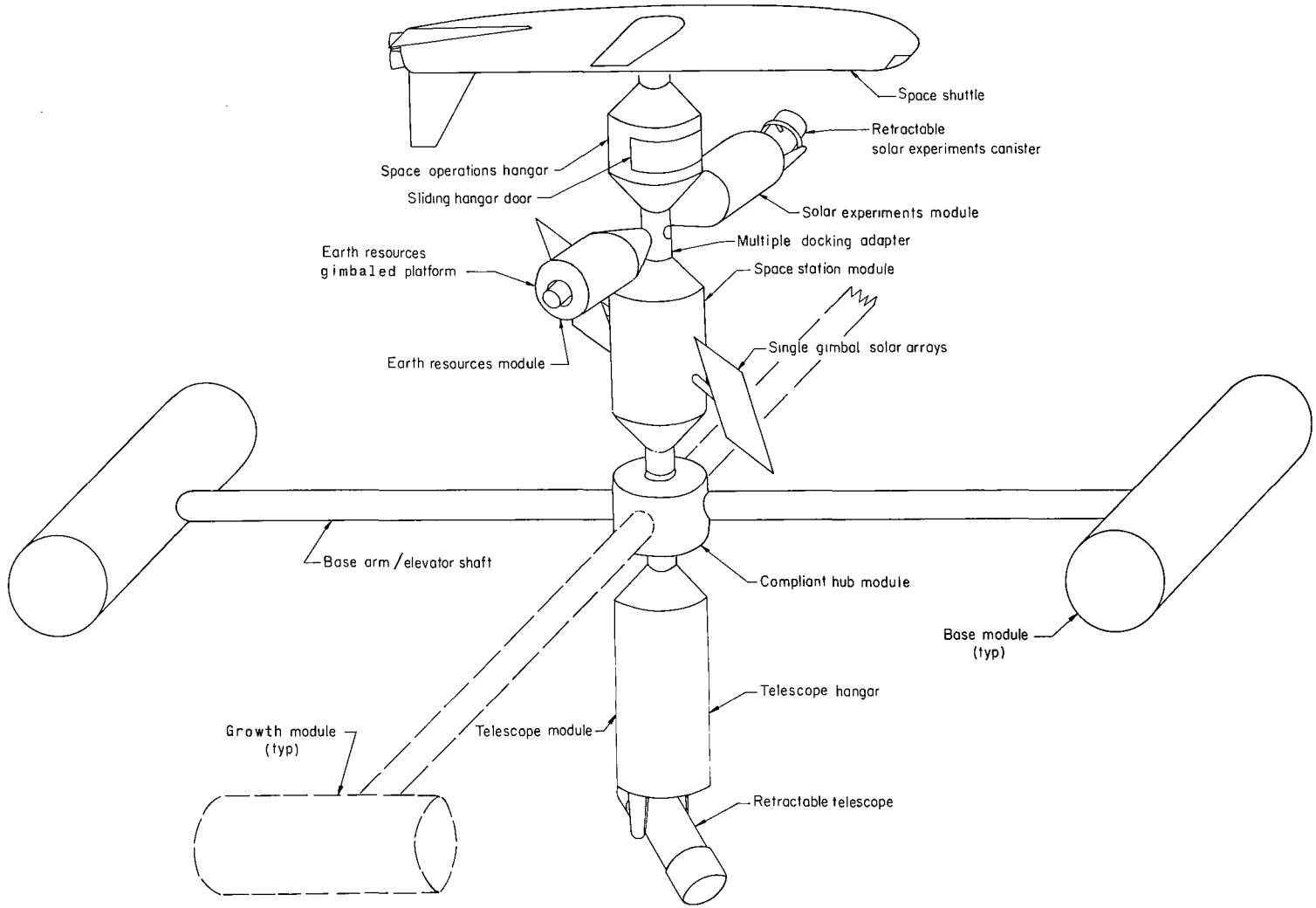

Figure 1.- Typical space base configuration.

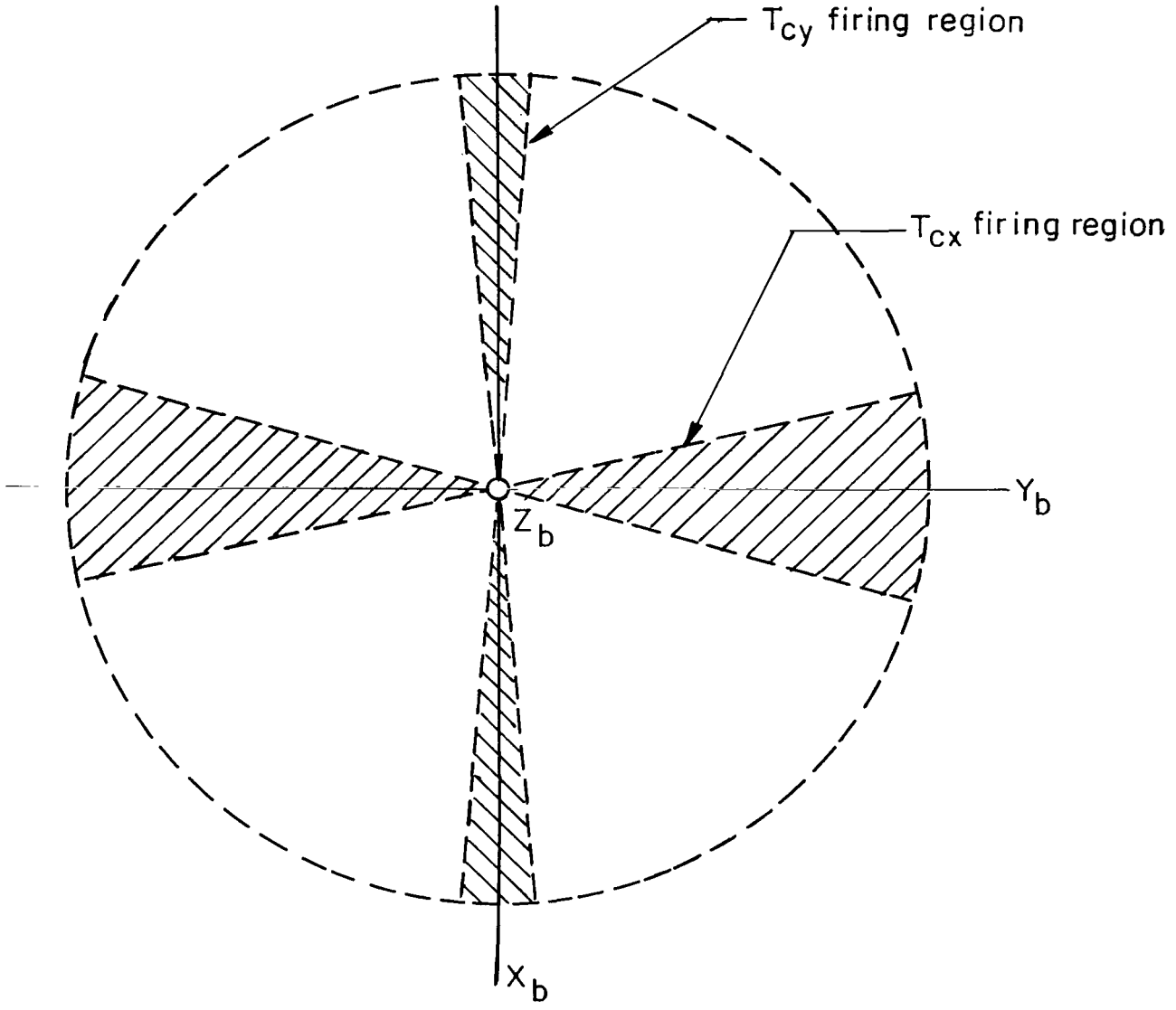

Figure 2.- Typical reaction jet firing regions.

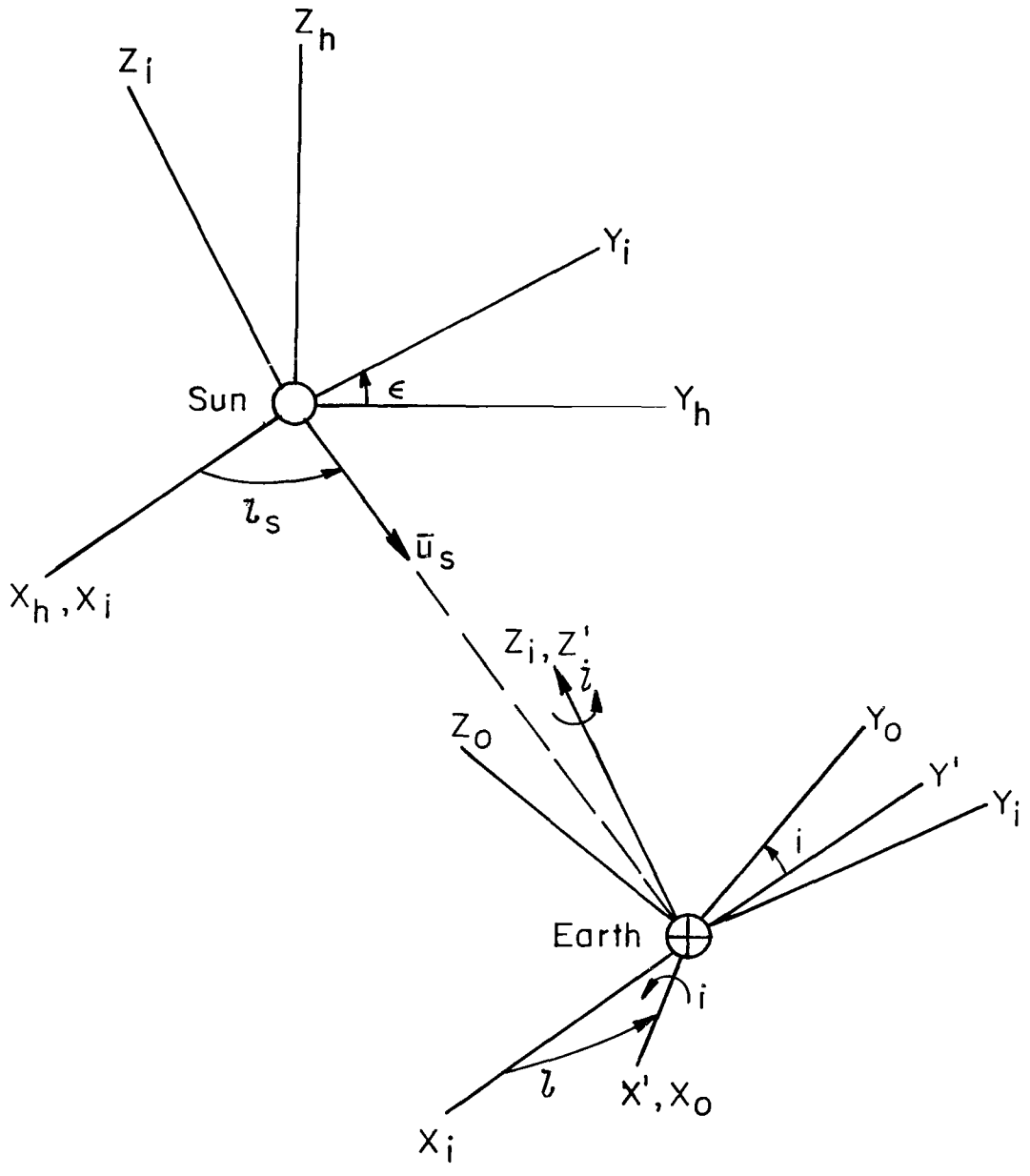

Figure 3.- Basic reference coordinate systems.

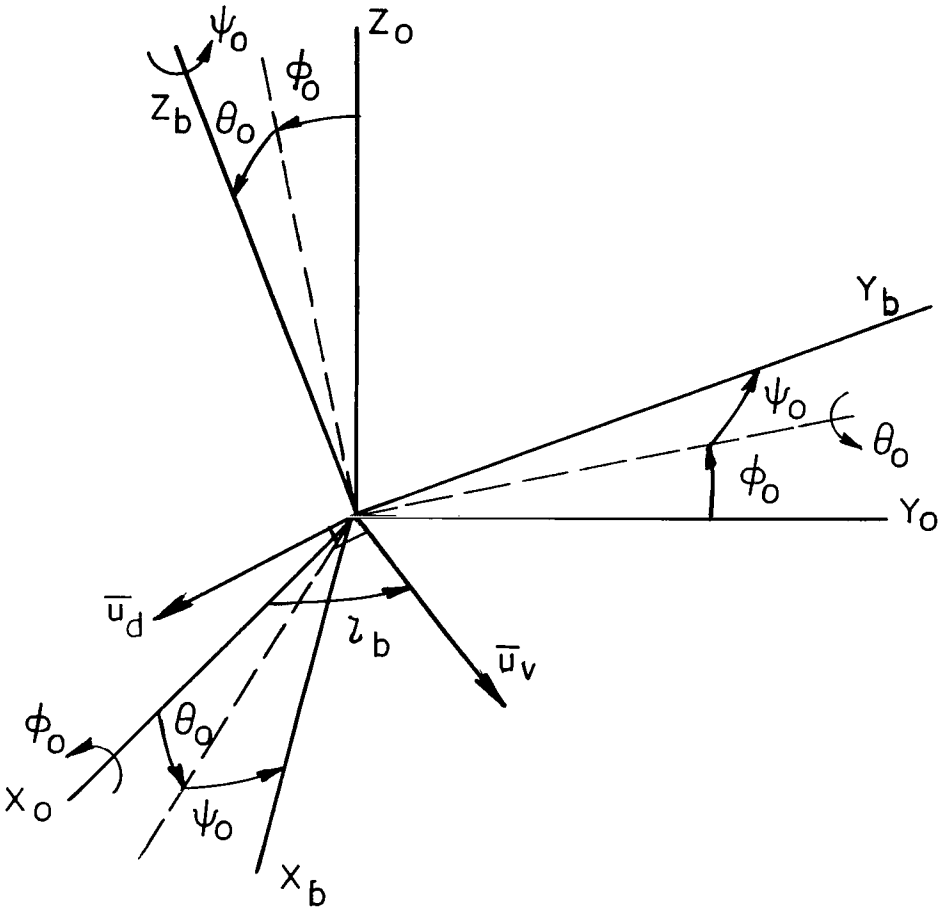

Figure 4.- Space-base—orbit-plane coordinates.

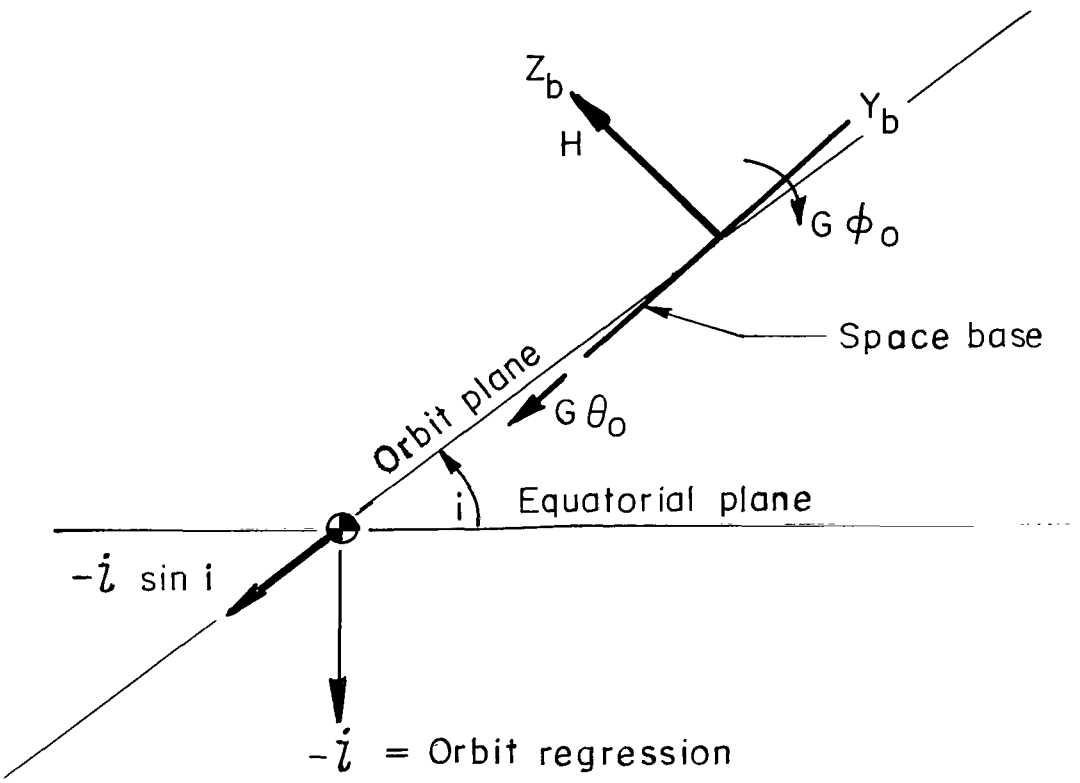

Figure 5.- Space base free body diagram.

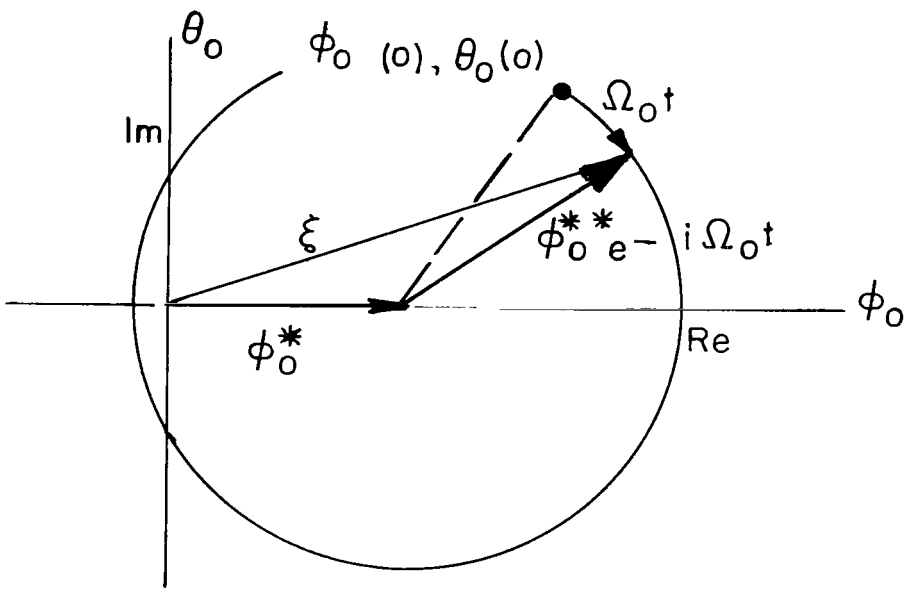

Figure 6.- Complex plane representation of momentum vector coning.

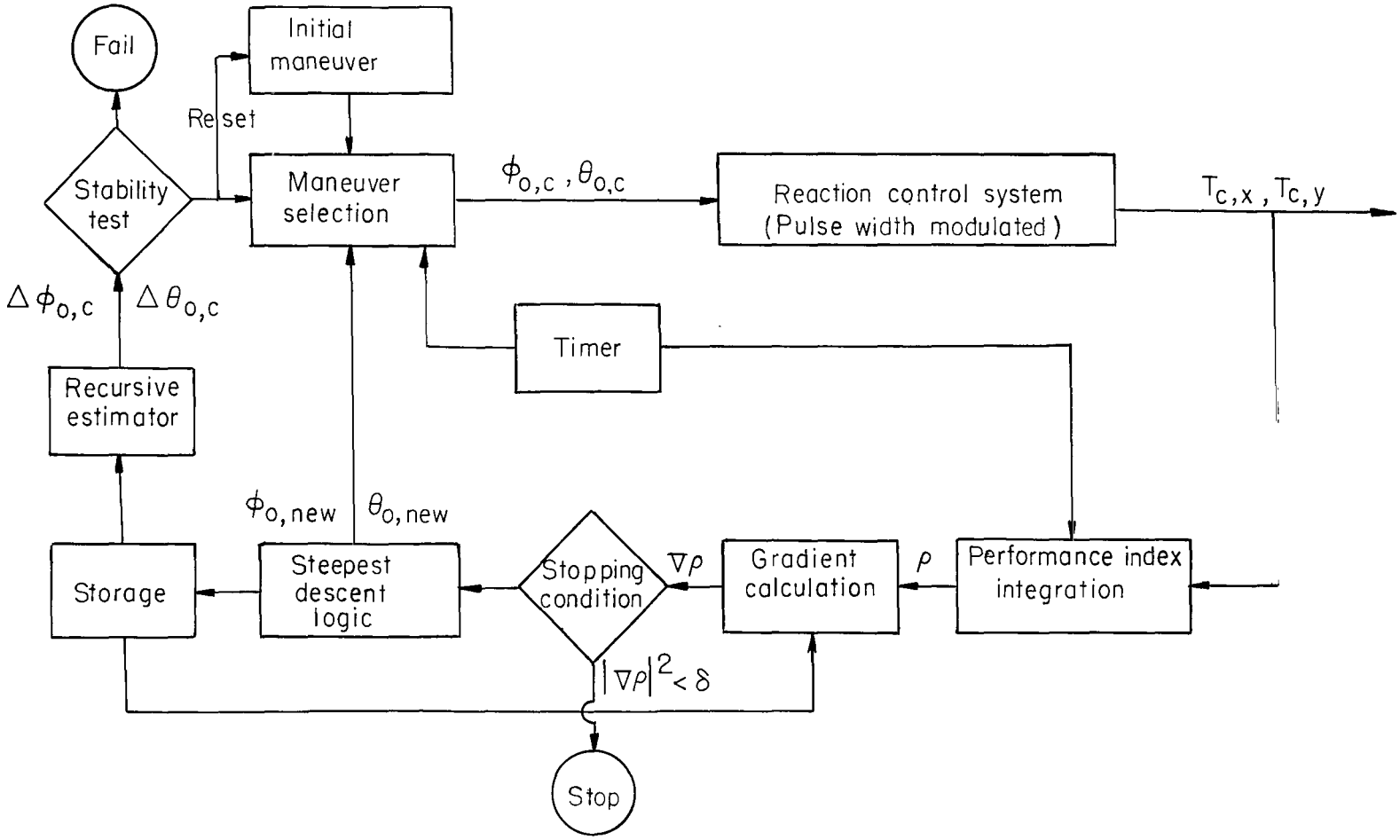

Figure 7.- Adaptive controller block diagram.

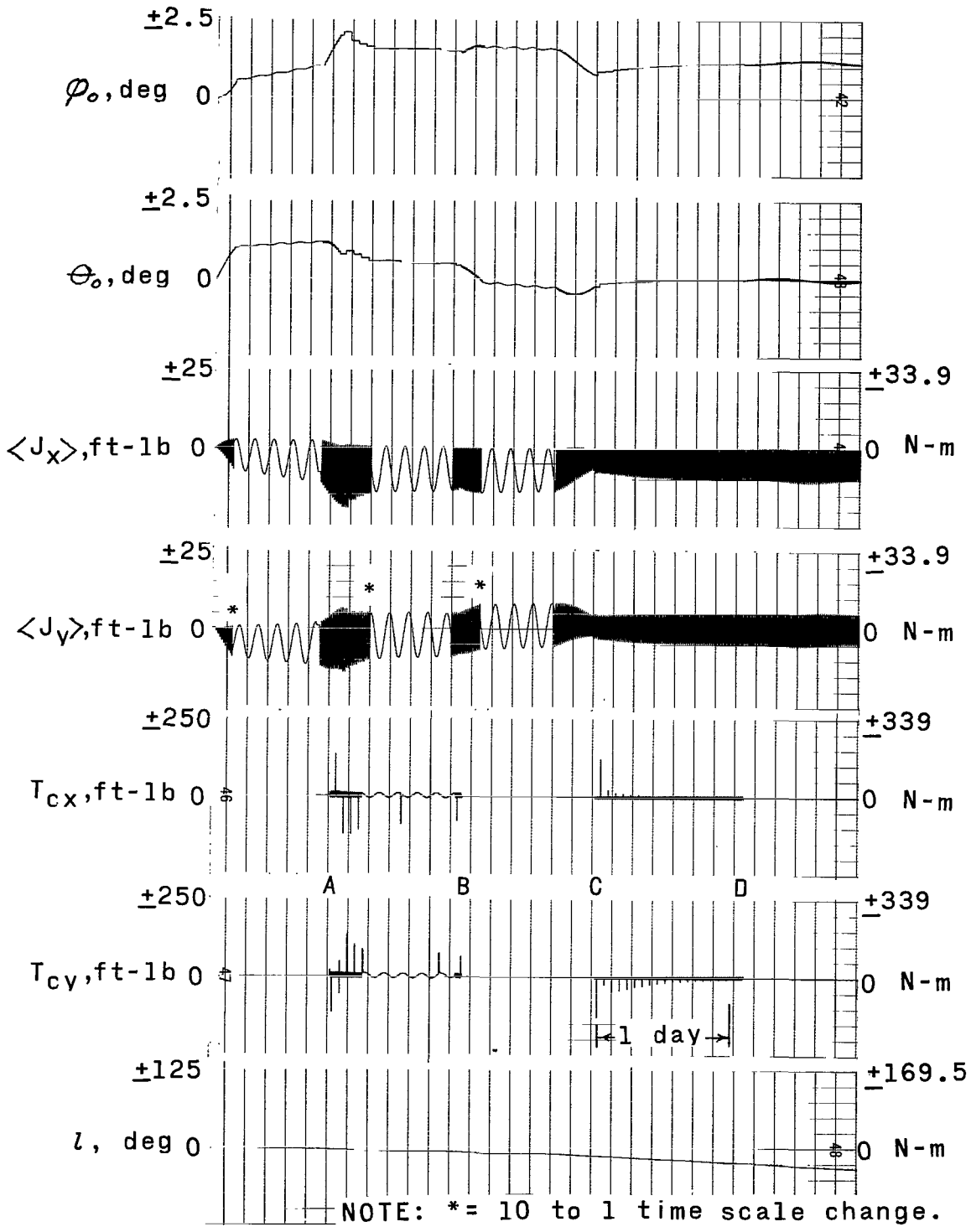

Figure 8.- Simulation time history traces.

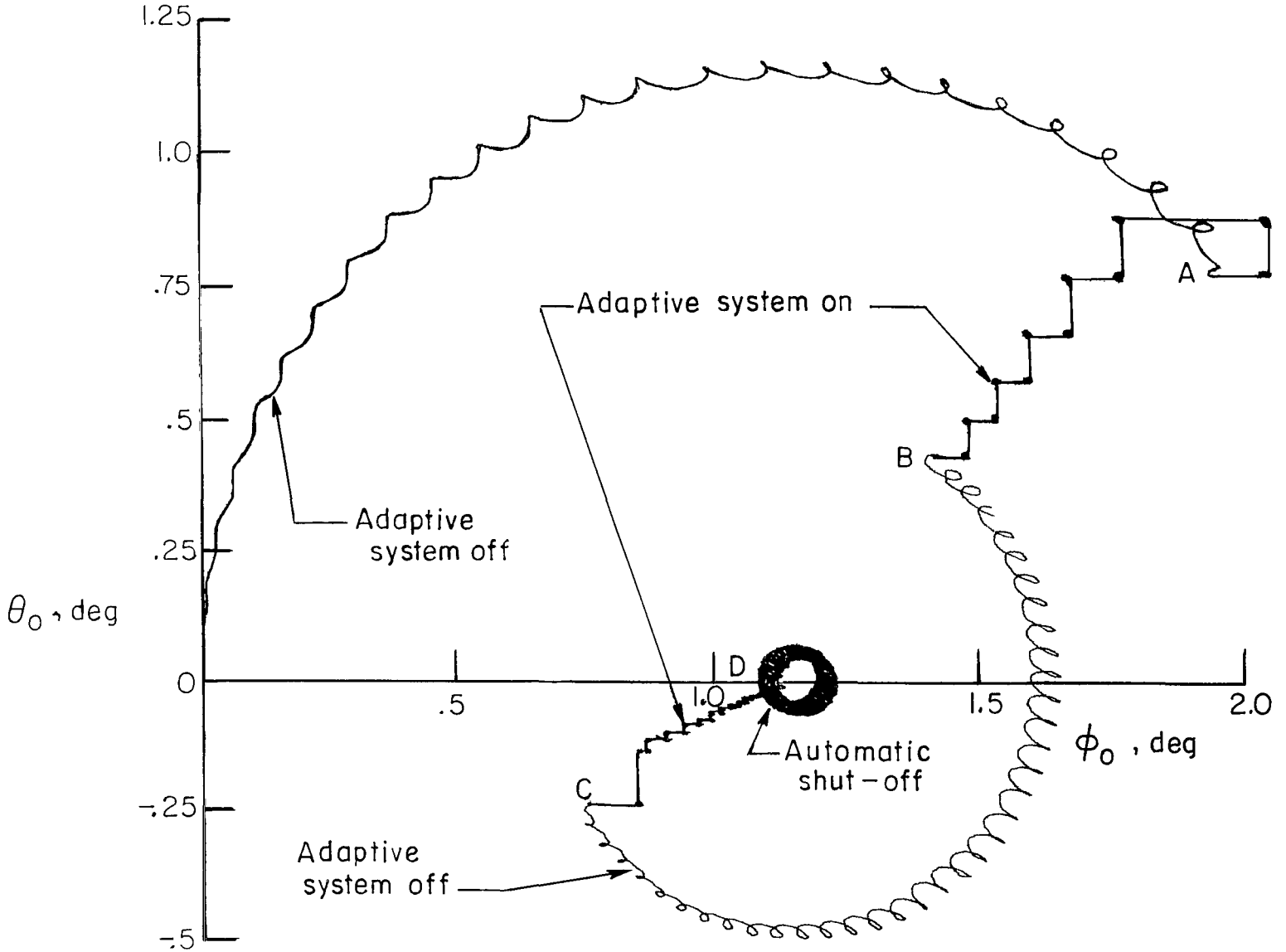

Figure 9.- Cross-axis trace for 0.2 configuration.

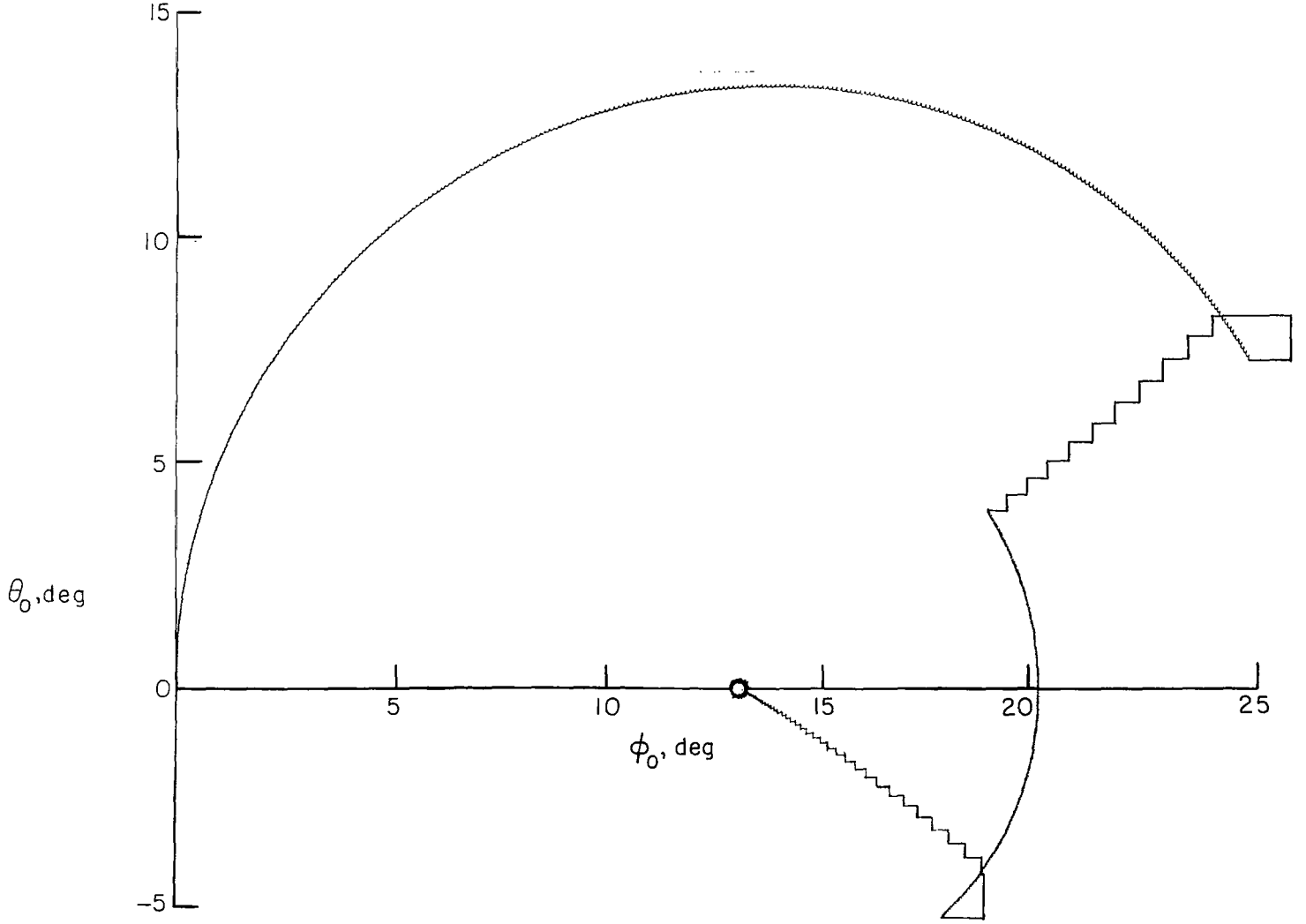

Figure 10.- Cross-axis trace for design configuration.

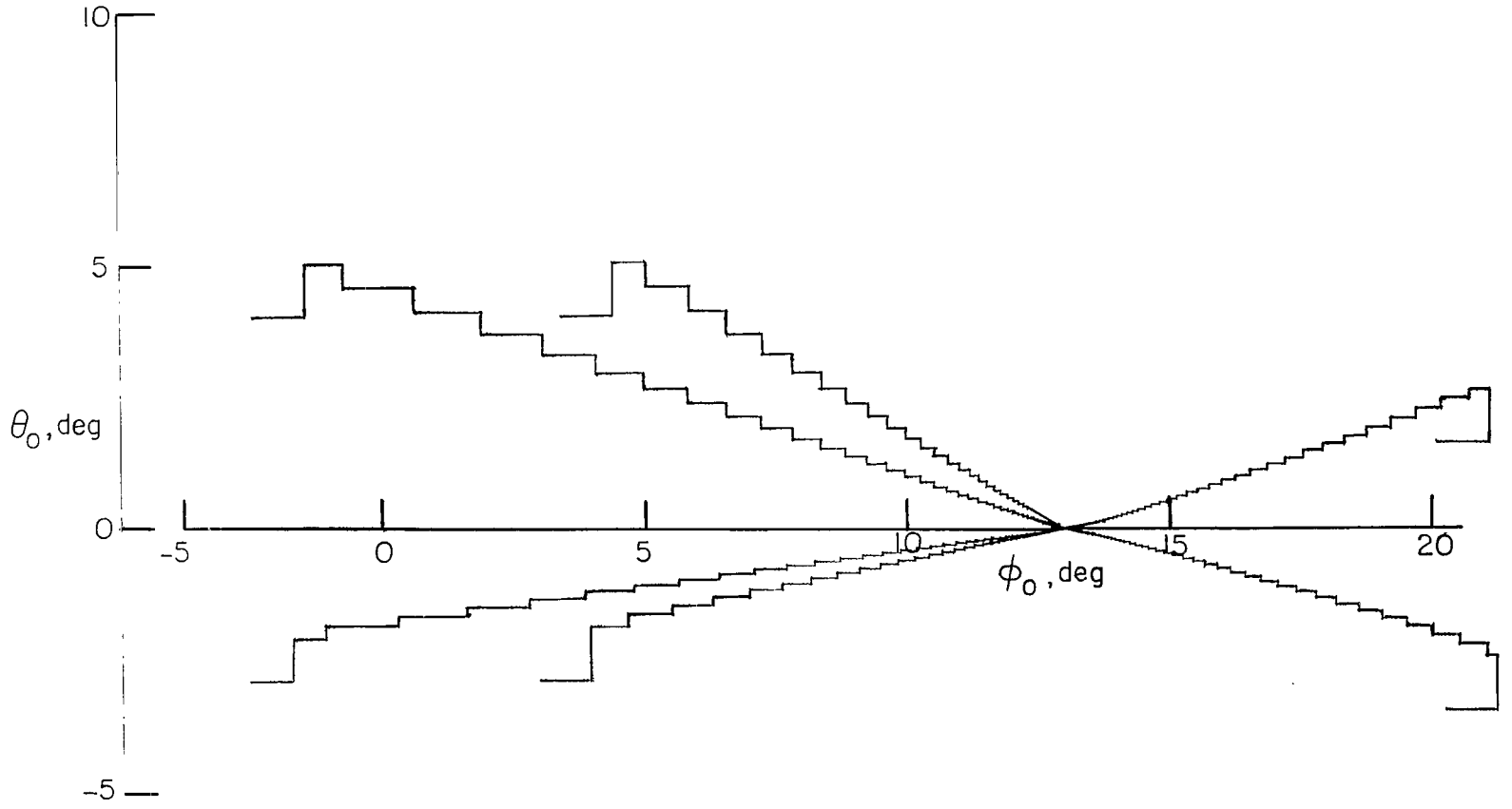

Figure 11.- Design configuration acquisition from various initial conditions.

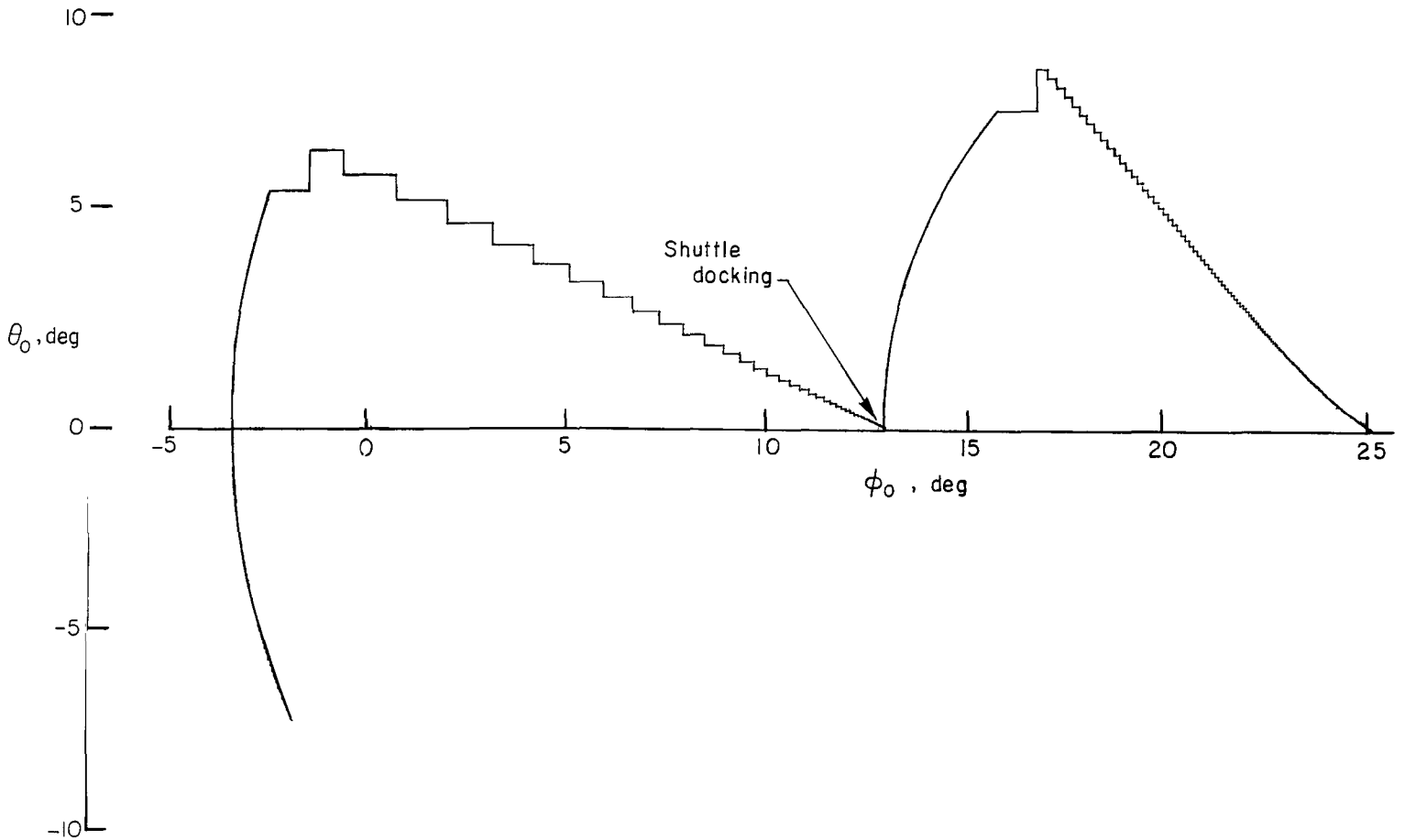

Figure 12.- Cross-axis trace for shuttle docking.

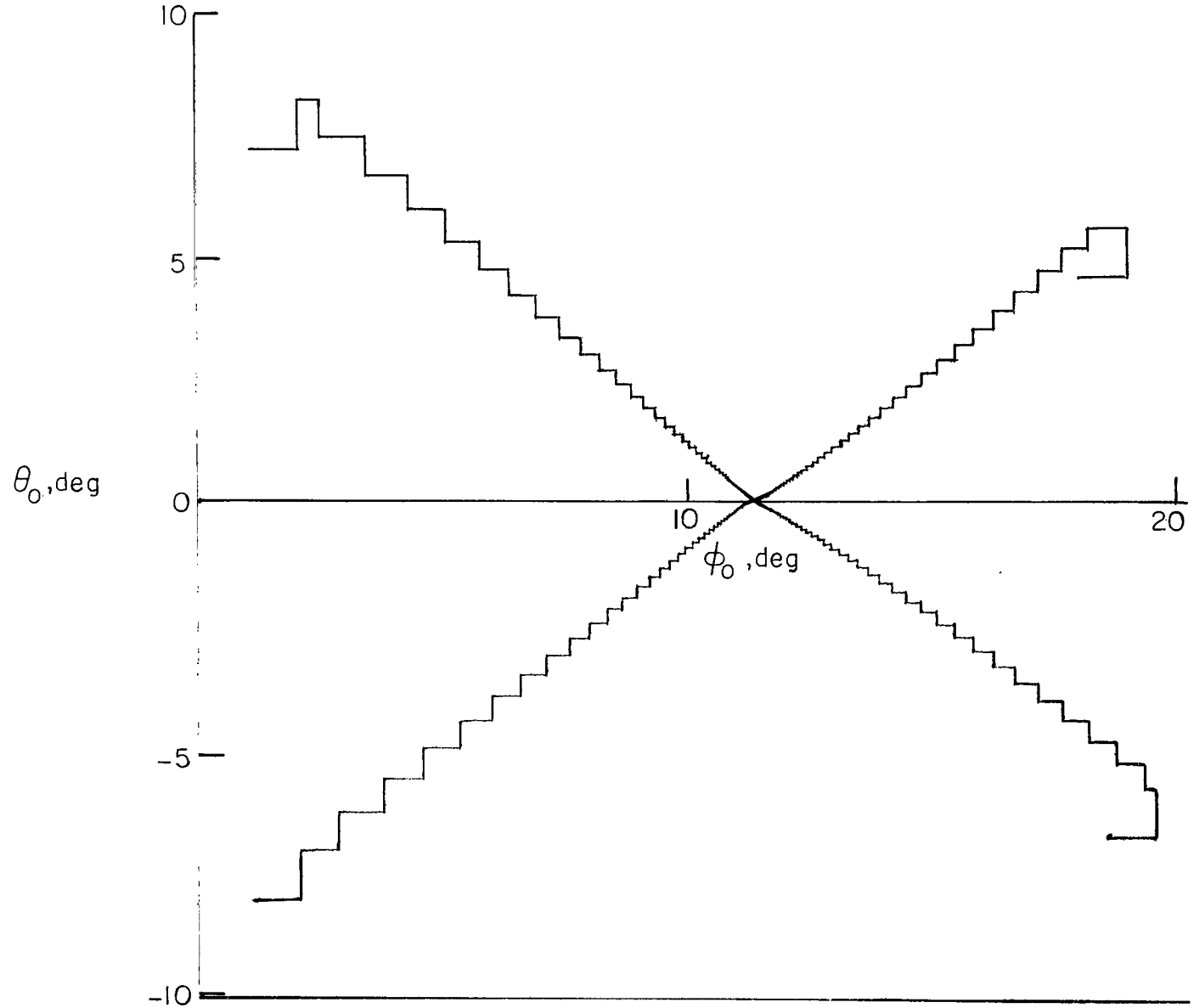

Figure 13.- Growth version acquisition from various initial conditions.

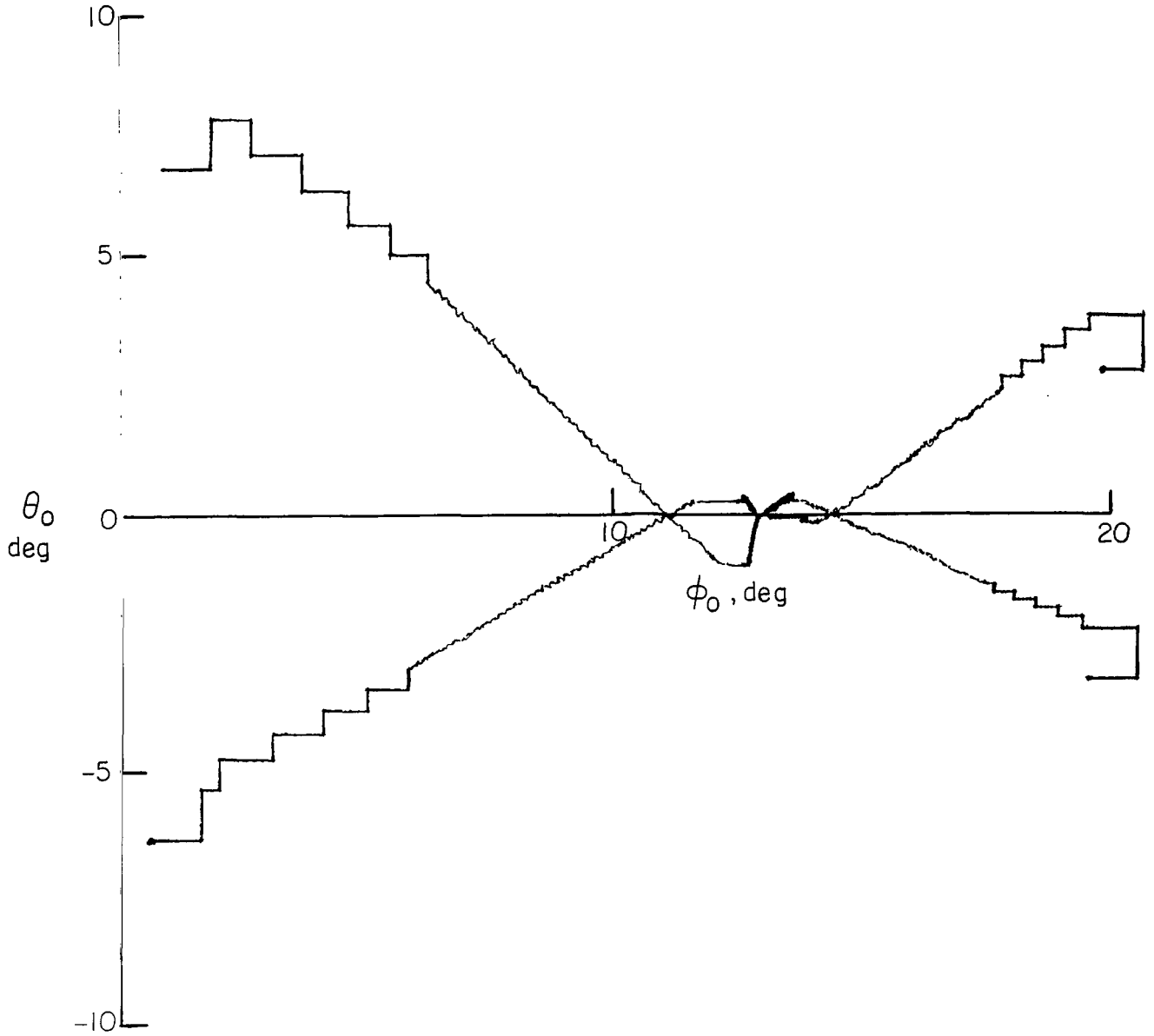

Figure 14.- Cross-axis plot of design configuration with learning logic.

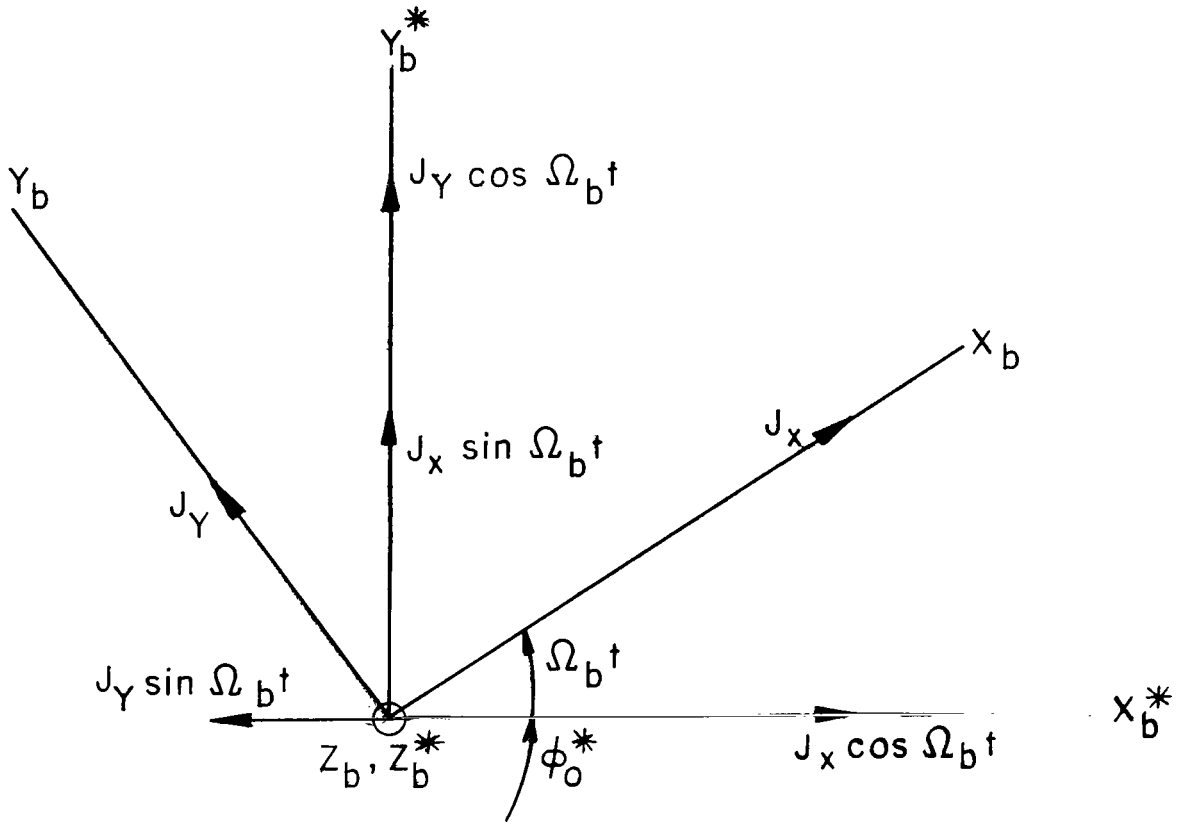

Figure 15.- Gravity gradient torque components.

NASA-Langley, 1970 —— 31 L-7157

"The aeronautical and space activities of the United States shall be conducted so as to contribute . . . to the expansion of human knowledge of phenomena in the atmosphere and space. The Administration shall provide for the widest practicable and appropriate dissemination of information concerning its activities and the results thereof."

—NATIONAL AERONAUTICS AND SPACE ACT OF 1958

NASA SCIENTIFIC AND TECHNICAL PUBLICATIONS

TECHNICAL REPORTS: Scientific and technical information considered important, complete, and a lasting contribution to existing knowledge.

TECHNICAL NOTES: Information less broad in scope but nevertheless of importance as a contribution to existing knowledge.

TECHNICAL MEMORANDUMS: Information receiving limited distribution because of preliminary data, security classification, or other reasons.

CONTRACTOR REPORTS: Scientific and technical information generated under a NASA contract or grant and considered an important contribution to existing knowledge.

TECHNICAL TRANSLATIONS: Information published in a foreign language considered to merit NASA distribution in English.

SPECIAL PUBLICATIONS: Information derived from or of value to NASA activities. Publications include conference proceedings, monographs, data compilations, handbooks, sourcebooks, and special bibliographies.

TECHNOLOGY UTILIZATION PUBLICATIONS: Information on technology used by NASA that may be of particular interest in commercial and other non-aerospace applications. Publications include Tech Briefs, Technology Utilization Reports and Notes, and Technology Surveys.

Details on the availability of these publications may be obtained from:

SCIENTIFIC AND TECHNICAL INFORMATION DIVISION

NATIONAL AERONAUTICS AND SPACE ADMINISTRATION

Washington, D.C. 20546